

Right Ventricle Shape and Contraction Patterns and Relation to Magnetic Resonance Imaging Findings

Jan Fritz, MD,*† Meiyappan Solaiyappan, BEngg, BE,* Harikrishna Tandri, MD,‡
Chandra Bomma, MD,‡ Ahmet Genc, MS,† Claus D. Claussen, MD,†
João A. C. Lima, MD,*‡ and David A. Bluemke, MD, PhD*‡

Objective: To analyze and to describe the shape and contraction of the normal right ventricle (RV) as visualized by magnetic resonance imaging (MRI).

Methods: Thirty normal volunteers were imaged using cine MRI in axial, short-axis, and long-axis planes. The shape and contraction of the RV were qualitatively evaluated. Quantitative evaluation of RV shape was performed by calculating the angle subtended between the planes of horizontal long-axis view (HLA) and axial view and the RV base-to-apex distance. Multiplanar reformation was used to visualize changes between corresponding views.

Results: The spectrum of major RV shape (wedge, box, and round) was more variable on axial images (17%, 43%, and 23%, respectively) than on HLA images (63%, 20%, and 0%, respectively). Focal outpouching of the RV free wall was more frequent on the axial view than on the HLA view. The subtended plane angle and base-to-apex distance showed statistically significant dependence indicative of an artificially foreshortened RV in the axial view with a direct influence on RV variations.

Conclusions: With increasing subtended angles, variation of the normal RV appearance is substantially higher on axial views compared with HLA views.

(*J Comput Assist Tomogr* 2005;29:725–733)

The right ventricle (RV) is frequently assessed qualitatively when evaluating cardiomyopathies. Understanding right ventricular shape and function is particularly important in the diagnosis of intrinsic disease of the RV, such as arrhythmogenic right ventricular dysplasia (ARVD),^{1–3} as well as in pulmonary hypertension and congenital heart disease.⁴

The shape of the RV is anatomically complex and difficult to characterize using cross-sectional imaging. The

RV can be divided into 1) an inflow region, consisting of the tricuspid valve, chordae tendineae, and papillary muscles; 2) the heavily trabeculated myocardium; and 3) a smooth myocardial right ventricular outflow tract (RVOT) that continues into the pulmonary trunk.^{5–7}

Magnetic resonance imaging (MRI) is commonly used for assessment of RV morphology and function.^{6,8} Different strategies for identifying optimal imaging planes for the RV have been developed over time but have not been standardized.⁹ Because the RV is infrequently studied compared with the left ventricle, determining pathologic findings versus findings related to normal variations or imaging technique may be difficult.

The purpose of this study was to determine the normal appearance of the RV by MRI in a study of 30 healthy volunteers. In particular, we sought to characterize the influence of the orientation of the heart on variations in the shape and contraction of the RV that may otherwise be mistaken for disease.

METHODS

Study Population

Thirty healthy white volunteers (12 female, 18 male, mean age: 32.6 ± 8.6 years) were recruited by advertisements through flyers and postings within our university (Table 1). Exclusion criteria were contraindications to MRI and diseases affecting the cardiovascular system. The study was approved by our institutional review board, and informed consent was obtained from all volunteers.

The volunteers were screened initially by telephone interview with a brief questionnaire, which included cardiac risk factors like hypertension, smoking history, family history of sudden death, symptoms such as history of syncope or chest pain, and current medication use. Before the MRI evaluation, 12-lead electrocardiography was performed on all subjects. Based on our evaluation before MRI, all volunteers seemed to be free of cardiovascular disease.

Acquisition Protocol

Magnetic resonance imaging was performed using a dedicated cardiovascular 1.5-T scanner (CV/I; General Electric Medical Systems, Waukesha, WI) equipped with 40-mT/m gradients. Imaging was performed with the patient in the supine position with a 4-element phased-array surface coil as

Received for publication May 5, 2005; accepted July 18, 2005.

From the *Russell H. Morgan Department of Radiology and Radiological Science, Johns Hopkins University School of Medicine, Baltimore, MD; †Department of Diagnostic Radiology, Eberhard-Karls-University, Tuebingen, Germany; and ‡Division of Cardiology, Johns Hopkins University School of Medicine, Baltimore, MD.

Reprints: David A. Bluemke, MRI Room 143 (Nelson Basement), The Johns Hopkins Hospital, 600 North Wolfe Street, Baltimore MD 21287 (e-mail: dbluemke@jhmi.edu).

Copyright © 2005 by Lippincott Williams & Wilkins

TABLE 1. Normal Volunteer Characteristics

Sex (M/F)	Age (y)	LV-EDV (mL)	LV-ESV (mL)	LV-SV (mL)	LV-EF (%)	RV-EDV (mL)	RV-ESV (mL)	RV-SV (mL)	RV-EF (%)
18/12	32.6 ± 8.6	155 ± 19.7	62 ± 12.4	93 ± 15.6	60 ± 8.3	161 ± 16.5	65 ± 13.6	96 ± 18.5	59 ± 8.6

EDV indicates end-diastolic volume; EF, ejection fraction; ESV, end-systolic volume; F, female; LV, left ventricle; M, male; RV, right ventricle; SV, stroke volume.

a receiver. Images were obtained during breath holding at end-expiration (resting lung volume) using electrocardiographic gating. For cine imaging, a segmented k-space steady-state free precession pulse sequence (FIESTA; General Electric Medical Systems) was used (repetition time/echo time/flip angle of 3.5–3.7 milliseconds/1.1–1.2 milliseconds/45°, 256 × 192 matrix, 10–12 views per segment, and temporal resolution of 35–44 milliseconds). After obtaining scout images, a series of 8–12 short-axis images and 6–10 axial cine images was obtained covering the RV and left ventricle. Axial images were taken perpendicular to the long axis of the body. The slice thickness was 8 mm, with 2-mm spacing between slices. In addition, horizontal long-axis (HLA; “4-chamber”) and RV vertical long-axis images were obtained.⁹

Image Evaluation

Cine images were evaluated using commercially available analysis software (MASS, version 4.1; MEDIS, Leiden, The Netherlands) on a workstation (Advantage Windows; General Electric Medical Systems). Measurement of right and left ventricular volumes were performed on short-axis images.¹⁰ For measurement of the distance between the tricuspid valve and apex (base-to-apex distance), the measurement tool from MASS was used.

The shape of the RV was evaluated on axial and HLA images by 2 experienced observers independently. Based on our prior experience with RV analysis and for the purposes of qualitative classification, 3 major shapes of the RV were identified (wedge shaped, box shaped, and round shaped; Figs. 1, 2):

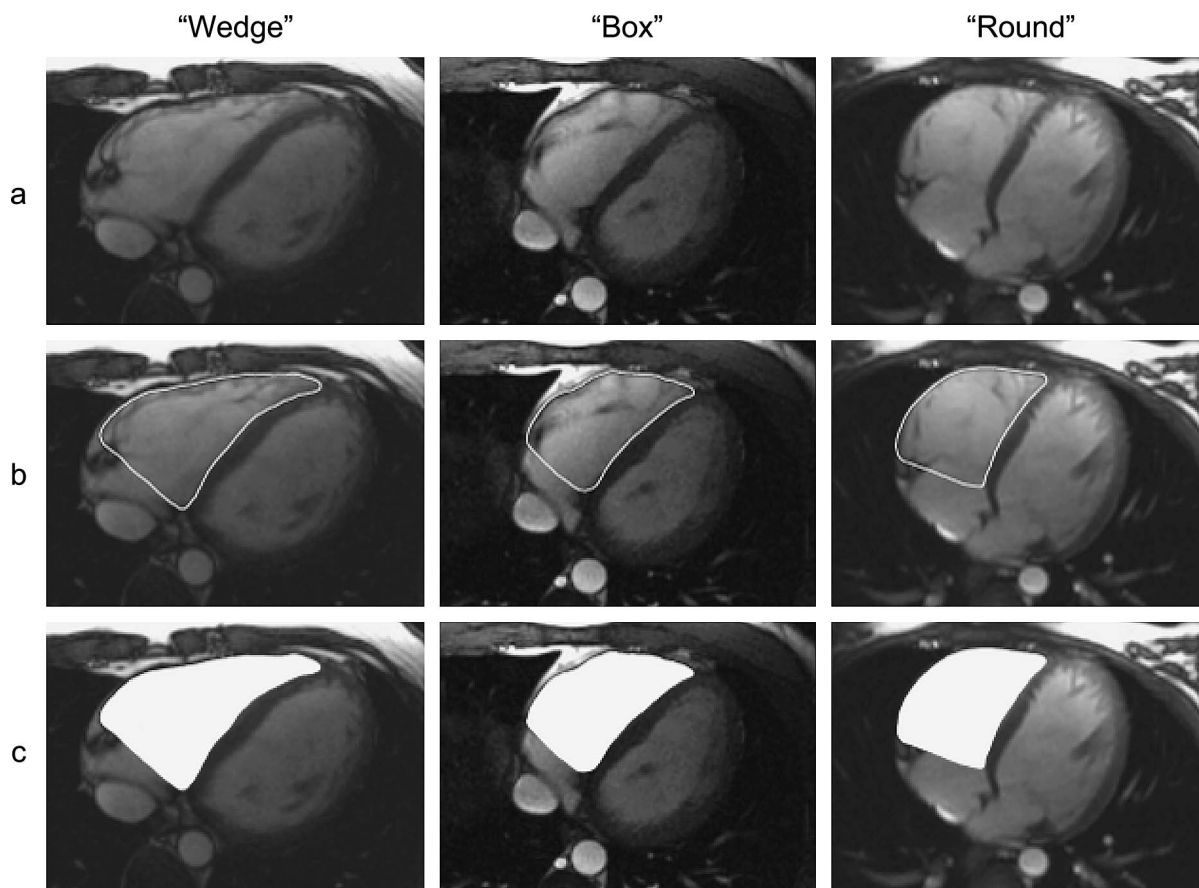


FIGURE 1. End-diastolic axial MRI scans (repetition time/echo time/flip angle of 3.7 milliseconds/1.2 milliseconds/45°) of 3 different patients demonstrate 3 major right ventricular shapes: wedge-shaped RVs (left column), box-shaped RVs (middle column), and round-shaped RVs (right column). Each row demonstrates 1) the original image, 2) the contour trace of the RV, and 3) the solid area of the RV.

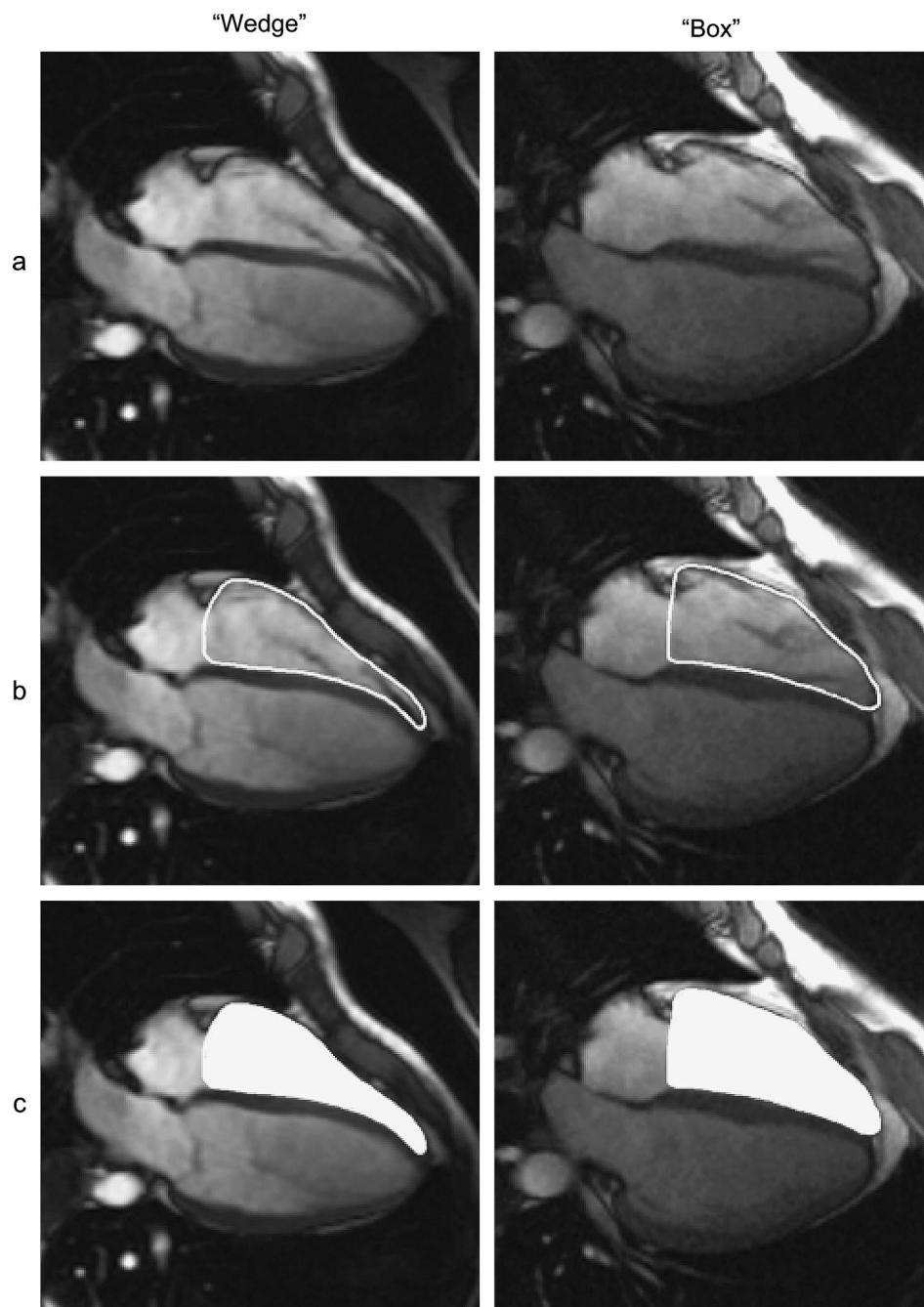


FIGURE 2. End-diastolic HLA MRI scans (repetition time/echo time/flip angle of 3.7 milliseconds/1.2 milliseconds/45°) demonstrate the 2 major right ventricular shapes: wedge-shaped RVs (left column) and box-shaped RVs (right column). Each row demonstrates 1) the original image, 2) the contour trace of the RV, and 3) the solid area of the RV.

- A wedge-shaped RV was characterized by a relatively linear anterior free wall without bulging at the middle to apical RV free wall location. This “straight” RV free wall resulted in a “wedge” or triangular-shaped RV.
- A box-shaped RV was characterized by a nonlinear anterior free wall that showed an anterior bulge at the middle to apical RV free wall location or a “sharp bend.” This resulted in a squared off or box-shaped RV.
- A round-shaped RV was characterized by a continuously convex curved anterior free wall of the RV without straight segments or focal outpouching on axial images. The

curvature of the RV free wall in this configuration, together with the normal left ventricle curvature, combined to create the overall form of a round heart on axial images.

When the 2 reviewers disagreed, the shape was classified as intermediate between the 2 major categories (ie, wedge-to-box shaped and box-to-round shaped).

Contraction patterns of the RV free wall were assessed in cine mode. Specifically, any focal “bulging” of the anterior RV wall at end-diastole/systole or appearing during systolic contraction was identified (Fig. 3). Disagreements by the 2 independent reviewers were resolved by consensus.

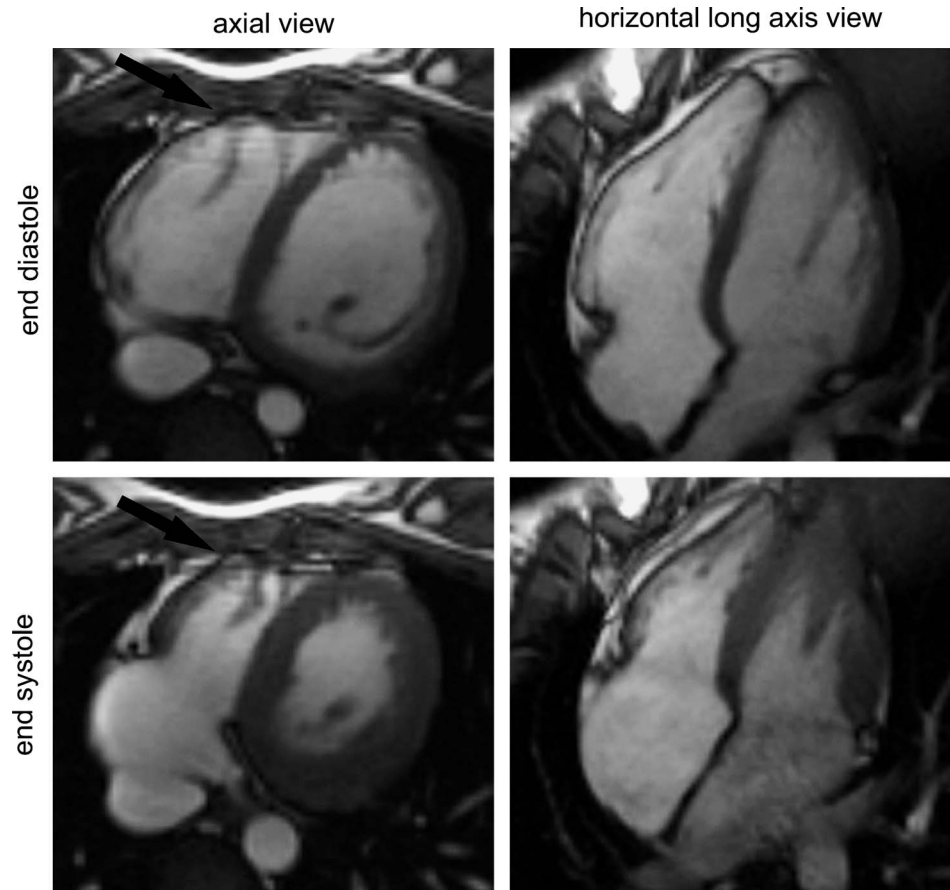


FIGURE 3. Corresponding axial and HLA MRI scans (repetition time/echo time/flip angle of 3.7 milliseconds/1.2 milliseconds/45°) within the same volunteer with a subtended plane angle of 38°. The image set demonstrates a normal contraction pattern of the right ventricular free wall on the HLA view and a variant contraction pattern on axial images with apparent end-diastolic and systolic bulging (black arrows) of the apical third of the right ventricular free wall.

Determination of Angles Between Axial and Horizontal Long-Axis Planes

To provide a quantitative assessment of the differences in shape of the RV on axial and HLA views, we calculated the subtended angle between the 2 image plane orientations (Fig. 4). The subtended angle between 2 planes (nonparallel) represents the angle by which one plane is rotated from the other about their common line of intersection. The information used to calculate the subtended angle was provided in the Digital Imaging and Communications in Medicine standard (DICOM) header of the MRI scan by a pair of vectors. From this pair, the subtended angle was computed by vector cross-product (Appendix).

Multiplanar Reconstruction

To visualize changes of RV appearance between the HLA and axial views in each volunteer directly, Voxtool software (Voxtool, 3.0.58d; General Electric Medical Systems) was used on the Advantage Windows workstation. A 3-dimensional volume of the heart was generated from the stack of axial images. From this 3-dimensional volume, a vertical long-axis view of the RV was prescribed. Then, an 8-mm-thick imaging slice was stepwise rotated at increments of 1° into the axial plane based on the calculated subtended angle for each volunteer. With each rotation step, the imaging plane was reconstructed for cine transition (Fig. 5).

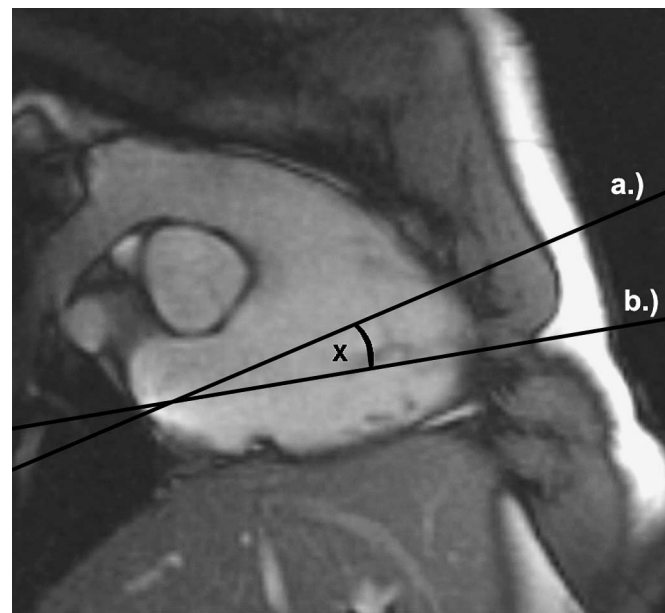


FIGURE 4. Right ventricle vertical long-axis MRI scan (repetition time/echo time/flip angle of 3.7 milliseconds/1.2 milliseconds/45°) with corresponding axial image plane (A) and HLA image plane (B). The orientation of the HLA image plane and that of the subtended image plane angle (X) are patient specific, depending on the orientation of the heart in the body.

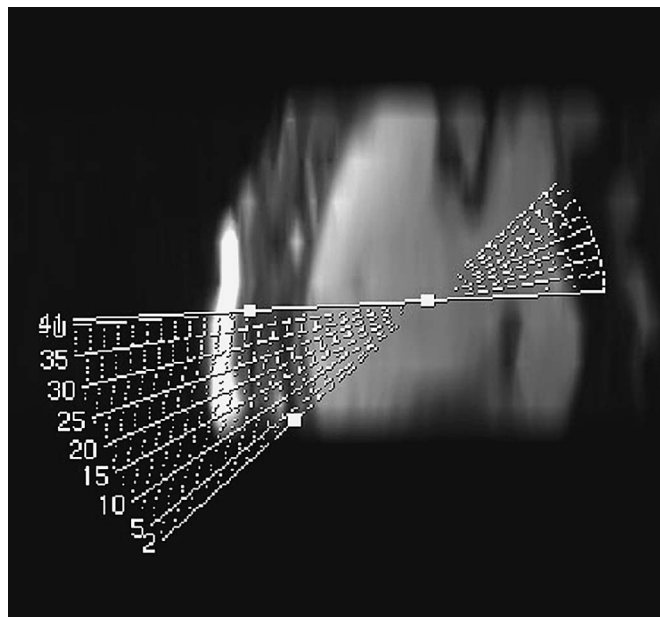


FIGURE 5. Right ventricular vertical long-axis MRI scan (3-dimensional volume digital reconstruction) showing the prescribed HLA plane (slice 1) and axial plane (slice 41) for multiplanar digital reconstruction. Slices 2 to 40 demonstrate the stepwise rotation in increments of 1° in the axial plane based on the calculated subtended angle for each volunteer.

Statistical Analysis

The mean and first standard deviations were derived for the right and left ventricular volumes and ejection fractions. To compare the 2 groups, the Mann-Whitney *U* test was used. A nonparametric correlation was used to determine the extent and direction of association between the base-to-apex-distance ratio and subtended angle between HLA and axial views.¹¹ *P* values less than 0.05 were regarded as statistically significant. All statistical analyses were carried out using SPSS version 12.0 software (SAS Institute, Cary, NC).

RESULTS

Results of Shape Classification

On axial images, the most frequent RV shape was a box in 13 (43%) of 30 normal volunteers. The round shape was present in 7 (23%) of 30 cases, followed by the wedge shape in 5 (17%) of 30 cases. Intermediate wedge-to-box-shaped contours were found in 3 (10%) of 30 cases, and intermediate box-to-round-shaped contours were found in 2 (7%) of 30 cases.

On the HLA view, the most frequent shape of the RV was a wedge in 19 (63%) of 30 cases, followed by a box shape in 6 (20%) of 30 cases. An intermediate wedge-to-box shape was seen in 5 (13%) of 30 cases. There were no round-shaped contours and no intermediate box-to-round-shaped contours seen on HLA views (Fig. 6). The frequencies of the 3 major RV shapes detected in transverse planes versus the axial plane were statistically significant (*P* < 0.05).

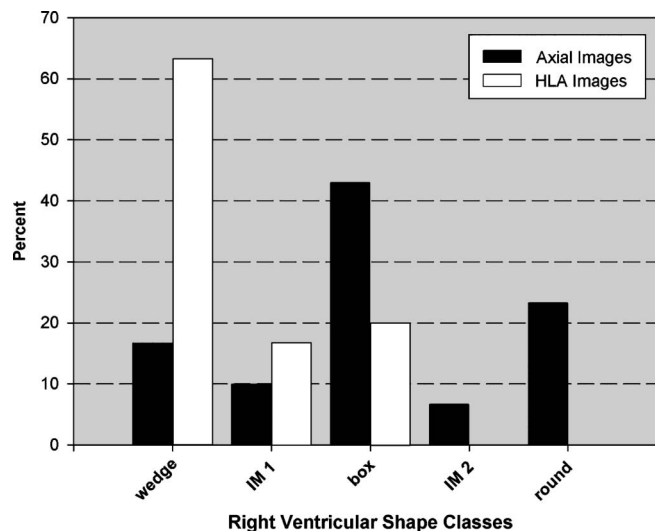


FIGURE 6. Distribution of right ventricular shape on axial MRI scans and HLA MRI scans. The diagram demonstrates increased variation of the RV shape appearance on axial MRI scans. In general, there was decreased variation of the RV shape on HLA MRI scans; in particular, there were no round-shaped RVs on the HLA view. IM1 indicates intermediate wedge-shaped box; IM2, intermediate round-shaped box.

Shape Changes Between Corresponding Imaging Planes

Based on the individual subtended angle between the HLA and axial plane, 3 patient groups were defined with subtended angles <30° (5 [16.7%] of 30 patients), 30°–40° (18 [60%] of 30 patients, and >40° (7 [23.3%] of 30 patients). Comparisons of RV shape class of paired HLA and axial views of the same volunteer were performed. There were no changes of RV shape class in cases with a subtended angle <30° (Fig. 8, movie 1). Changes between the HLA and axial views were only seen in volunteers with subtended angles >30°. In the group with subtended angles between 30° and 40°, RV shape class changed in 14 (77.8%) of 18 cases, and in the group with subtended angles >40° (see Fig. 8, movie 2), there was a change in classification of RV shape in all cases.

Furthermore, on axial images, no round shapes were seen in the group with angles <30° and no wedge shapes were seen in the group with angles >40°. In general, round RV shape increased as the subtended angle between the HLA and axial views increased.

Contraction Pattern

During systole, focal outpouching of the RV free wall (bulging) was seen on axial images in 19 (63.3%) of 30 cases. This bulging was always located in the apical third of the right ventricular free wall (see Fig. 3). On HLA views, however, focal bulging of the right ventricular free wall was only seen in 3 (10%) of 30 cases. In volunteers with subtended angles <30°, no bulging was diagnosed on the axial or HLA view. In volunteers with subtended angles between 30° and 40°, bulging was diagnosed in 12 (66.7%) of 18 cases on axial images and in 2 (0.25%) of 18 cases on the HLA view. In 9 cases,

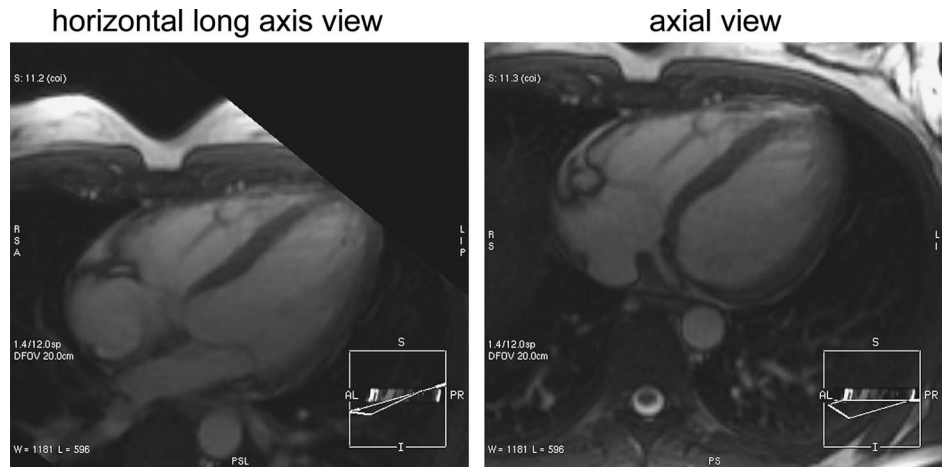


FIGURE 7. Movie images. Multiplanar reformation of 3-dimensional volumes generated from stacks of axial images of a patient with a subtended angle between the HLA images (left column) and axial images (right column) of 21°. Multiplanar reformation demonstrates that there is no change of RV shape class and no end-diastolic focal outpouching of the RV free wall (movie file 1).

bulging was present on axial views, whereas HLA views were diagnosed without bulging. In volunteers with a subtended angle >40°, bulging was always identified on axial images (7 [100%] of 7 cases) and in 1 case on the HLA view. In 6 (85.7%) of 7 cases with bulging on axial images, the HLA views were diagnosed as normal.

End-diastolic outpouching of the RV free wall was only seen on axial images (8 [44%] of 18 cases) in patients with subtended angles between 30° and 40°. Corresponding end-diastolic HLA images were found to be normal (see Fig. 3).

Dependency Between Horizontal Long-Axis and Axial Views

With the determined base-to-apex distance of HLA and axial views in each volunteer, a ratio of paired distances (base-to-apex distance of HLA view/base-to-apex distance of axial images) was calculated. This ratio and the subtended angles were negatively correlated ($r = -0.656, P < 0.001$; Fig. 9). Thus, increased downward (inferior) tilt of the cardiac apex of the heart in the chest causes relative foreshortening of the RV

in the axial plane because of the oblique orientation of the image plane. This finding contributes to the difference in RV appearance between HLA and axial views.

Multiplanar Reformation

Multiplanar reformation directly visualized changes in RV shape between the 2 imaging planes and the appearance of the focal outpouching of the RV free wall. This approach demonstrated the identified major RV shapes as part of a continuum extending from wedge over box to round RV shape in volunteers with increased subtended angles (Fig. 7). Furthermore, this approach revealed that the appearance and disappearance of end-diastolic focal outpouching of the anterior RV free wall were attributable to distinct portions of the RVOT that were increasingly visualized on the axial view with subtended angles between 30° and 40° compared with HLA views (see Fig. 8).

These findings confirm our results of the shape and contraction analysis. The RV appearance and variation are

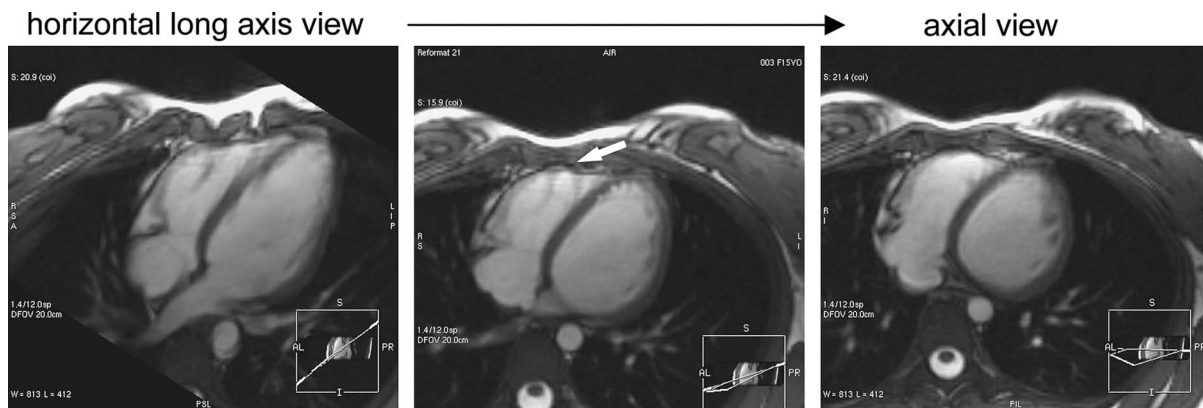


FIGURE 8. Movie images. Multiplanar reformation of 3-dimensional volumes generated from stacks of axial images of a patient with a subtended angle between HLA images (left column) and axial images (right column) of 41°. The multiplanar reformation demonstrates the appearance of end-diastolic focal outpouching of the RV free wall during transition attributable to the oblique visualization of a distinct region of the RVOT. It also demonstrates the disappearance of focal outpouching with the transition to a subtended angle of 41°. Finally, the shape changes to a round RV appearance on axial views as it is influenced by increased involvement of the RVOT (movie file 2).

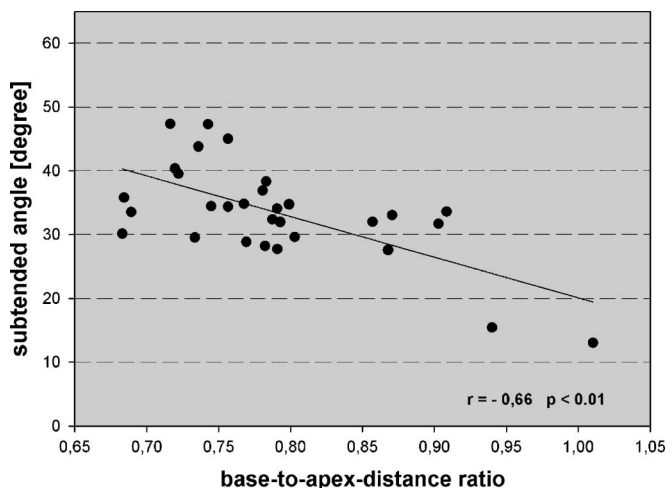


FIGURE 9. Correlation of base-to-apex-distance ratio (base-to-apex distance of HLA view images/base-to-apex distance of axial images) and subtended angles demonstrating a negative correlation ($r = -0.656$, $P < 0.001$). Thus, increased downward (inferior) tilt of the cardiac apex of the heart in the chest causes relative foreshortening of the RV in the axial plane because of the oblique orientation of the image plane. This potentially leads to the difference in RV appearance between HLA and axial views.

markedly influenced by the angle subtended between HLA and axial views accordingly.

DISCUSSION

Evaluation of the RV by cross-sectional imaging has been confounded by its complex shape and by the tendency to interpret RV contraction and shape in a manner similar to our understanding of the left ventricle. The left ventricle, however, is symmetric; thus, its function and shape are readily evaluated. Abnormalities of the RV are less common than pathologic conditions involving the left ventricle, and this likely further contributes to a lack of understanding of the normal and diseased state of the RV. The consequences of misinterpretation of the RV by MRI have been documented.¹²

In this report, we have provided the first qualitative description of normal variations in RV morphology as observed by MRI and have supported this by quantitative analysis of the variations in RV orientation in the chest. Angular variation in RV orientation in the chest is likely a continuous function; however, for purposes of classification and as an aid to understanding, we have described 3 major RV appearances on axial MRI.

In particular, the box-shaped RV is present in approximately 40% of normal individuals on axial images. This shape is characterized by a nonlinear anterior wall and was frequently associated with focal outpouching. This focal outpouching is easily mistaken for a regional wall motion contraction abnormality. Based on comparison with multiplanar reconstruction, end-diastolic focal outpouching on axial images is attributable to a distinct portion of the RVOT that is visualized depending on the individual orientation of the longitudinal heart axis.

Variation in shape of the RV was less on the HLA view compared with the axial view. The HLA view is independent because of its relative orientation to the heart axis.

Currently, the RV is frequently imaged in the axial plane by MRI as well as by computed tomography. In a referral setting of 50 patient examinations received from 43 institutions, a high degree of variability between MRI centers was identified for RV imaging: 59% of centers obtained axial images, 16% obtained sagittal images, 12% obtained short-axis images, 7% obtained coronal images, and 6% obtained long-axis images.¹³ Advantages of axial imaging include ease of prescription for the technologist and thorough visualization of the base of the RV, tricuspid valve, anterior free wall, and RVOT.

Contraction of the Normal Right Ventricle

On cine MRI, there was apparent bulging of the anterior RV wall during systole much more often (63.3%) on axial images than on HLA views (10%). On axial images, bulging was located in the apical third of the right ventricular free wall. A common site was close to the region where the fused complex consisting of the anterior papillary muscle, the moderator band, and the parietal band arises from the right ventricular free wall.^{6,7,14} With increased subtended angle, bulging could be seen on axial views even when it was not present on HLA views (84.2%), in agreement with a prior report by Sievers et al.¹⁴ In cases with subtended angles $>40^\circ$, systolic bulging was always seen on axial images. End-diastolic focal outpouching was only seen in cases with subtended angles from 30° to 40° . Thus, apparent bulging on axial views can be considered a normal finding, particularly when HLA views are unremarkable. This has important implications for the MRI diagnosis of ARVD, in which apparent bulging could be mistaken for a pathologic wall motion abnormality or structural defect.

Clinical Significance

In diseases such as ARVD, the RV is directly affected.^{15,16} In the diagnostic procedure of ARVD, MRI has evolved to a powerful tool^{3,6,17-21} that allows excellent assessment of structural and functional abnormalities of the RV.^{3,15,17,18,21} In addition to its ability to detect fatty and fibrofatty replacement of the myocardium,^{15,22} it is used for the assessment of global right ventricular dilatation and segmental right ventricular dilatation with or without aneurysms and bulging.²³ Magnetic resonance imaging of ARVD is currently performed without a “gold standard,” however.¹⁹ Magnetic resonance imaging findings have been demonstrated on axial images^{3,6,17,18} and on HLA images.²⁴ The description of normal right ventricular morphology with regard to plane orientation can add valuable information for distinction between normal and pathologic changes.

Our results emphasize the disadvantage of the axial plane in that it is not orthogonal relative to the inherent axis of the heart. The HLA view is a standardized image plane that is aligned along the long axis of the heart centered at the mid-ventricular level. Complete tomographic coverage of the RV in the long-axis plane has not been standardized,⁹ however, and

the relative value of a “stack” of parallel views in this plane has not been assessed.

The relation between base-to-apex distance ratio and subtended angle between axial and HLA views as well as the results of the transition in multiplanar reconstruction is consistent with the hypothesis that RV shape on axial images is markedly influenced by anatomic structures such as the RVOT. The degree of this influence depends on the individual orientation of the long axis of the heart and determines the portions of the RVOT visualized on axial MRI. This results in increased variability of RV shape and increased frequency of anterior free wall bulging of the RVs on axial images.

Limitations of Study

A sample size of 30 white volunteers recruited from an academic environment may not be representative of the general population. There may be additional insights if the sample size increases or if volunteers of different ancestry are examined. In addition, an assumption about the different RV shapes being associated with certain diseases cannot be made in this state of the observation.

The reported observations regarding RV shape and bulging are qualitative. The RV shapes we have described (wedge, box, and round) are primarily an aid to understanding these variations. We used “intermediate” categories for discrepant observations by the reviewers, and it is reassuring that only approximately 10% of RV shapes were placed in these intermediate categories. Furthermore, all cases of end-diastolic focal outpouching were previously correctly classified as box-shaped RVs. Nevertheless, experienced cardiovascular imagers recognize that there is a continuum of RV shapes, which contributes to potential misinterpretation of RV shape and function. Further efforts at quantitation of RV function, potentially using MRI tagging, may help to decrease physician variability in the diagnosis of RV health and disease using cross-sectional imaging. Unfortunately, the thin RV wall and its complex contraction pattern have thus far proven to be substantial problems to overcome using MRI tagging.

In conclusion, variations in RV shape are common, particularly on axial images, using MRI. Correlation with HLA views may be helpful to avoid misdiagnosis of structural and functional RV abnormalities.

APPENDIX

The subtended angle between 2 planes (nonparallel) represents the angle by which one plane is rotated from the other about their common line of intersection. Considering the oblique orientation of HLA view images, this would mean that the line of intersection would be at arbitrary angles with respect to major x - and y -axes. This required the use of 3-dimensional vector calculation to compute the subtended angle between planes using the normal vector.

The information about the normal plane is provided in the Digital Imaging and Communications in Medicine standard (DICOM) header of the MRI scan by a pair of vectors. These vectors represent the direction of the imaging plane's width (x_i , x_j , and x_k) and height (y_i , y_j , and y_k), which can be identified in the header as the image plane orientation.

From this pair, the normal plane is computed by the vector cross-product:

$$N(N_x, N_y, N_z) = [(x_j y_k - x_k y_j), (x_k y_i - x_i y_k), (x_i y_j - x_j y_i)]$$

Once the normal plane for each imaging plane is computed, the angle between the 2 vectors is determined from their vector dot product:

$$\text{Subtended Angle (in radians)} = \cos^{-1} \left(\frac{N_x^1 N_x^2 + N_y^1 N_y^2 + N_z^1 N_z^2}{|N^1| |N^2|} \right)$$

N^1 and N^2 are the normal plane vectors of axial and HLA images. For the axial images $N_x^1 = N_y^1 = 0$, the angle can also be computed as:

$$\text{Subtended Angle (in radians)} = \cos^{-1} \left(\frac{N_z^1 N_z^2}{|N^1| |N^2|} \right)$$

Because the subtended angle includes the total oblique rotation of the HLA view images, the subcomponents of this angle (ie, the angle with respect to the axial plane and the angle with respect to the coronal plane) were computed and included in the analysis for studying their individual contribution to the shape variations.

The angle with respect to coronal plane (ie, the plane of the body) is given by the following equation:

$$\text{Angle (in radians)} = \sin^{-1} \left(\frac{N_y}{|N|} \right)$$

The angle with respect to axial plane is given by the following equation:

$$\text{Angle (in radians)} = \tan^{-1} \left(\frac{N_x}{N_z} \right)$$

N is the normal plane of the HLA image. For presentation purposes, subtended angles were converted to degrees.

ACKNOWLEDGMENT

The authors acknowledge the support of NHLBI U01 HL65594-02, Johns Hopkins Subcontract, and the Johns Hopkins ARVD Center.

REFERENCES

1. Marcus FI. Is arrhythmogenic right ventricular dysplasia, Uhl's anomaly and right ventricular outflow tract tachycardia a spectrum of the same disease? *Cardiol Rev*. 1997;5:25–29.
2. Hoch DH, Rosenfeld LE. Tachycardias of right ventricular origin. *Cardiol Clin*. 1992;10:151–164.
3. Kayser HWM, van der Wall EE, Sivanathan MU, et al. Diagnosis of arrhythmogenic right ventricular dysplasia: a review. *Radiographics*. 2002;22:639–648.

4. Reddy GP, Higgins CB. Magnetic resonance imaging of congenital heart disease: evaluation of morphology and function. *Semin Roentgenol.* 2003;38:342–351.
5. Kirklin JW, Barratt-Boyes BG. *Cardiac Surgery.* New York: Churchill Livingstone; 1993.
6. White RD, Trohman RG, Flamm SD, et al. Right ventricular arrhythmia in the absence of arrhythmogenic dysplasia: MR imaging of myocardial abnormalities. *Radiology.* 1998;207:743–751.
7. Farb A, Burke AP, Virmani R. Anatomy and pathology of the right ventricle (including acquired tricuspid and pulmonic valve disease). *Cardiol Clin.* 1992;10:1–21.
8. Buxt LM. Radiology of the right ventricle. *Radiol Clin North Am.* 1999;37:379–400.
9. Cerqueira MD, Weissman NJ, Dilsizian V, et al. Standardized myocardial segmentation and nomenclature for tomographic imaging of the heart: a statement for healthcare professionals from the Cardiac Imaging Committee of the Council on Clinical Cardiology of the American Heart Association. *Circulation.* 2002;105:539–542.
10. Alfakih K, Plein S, Thiele H, et al. Normal human left and right ventricular dimensions for MRI as assessed by turbo gradient echo and steady-state free precession imaging sequences. *J Magn Reson Imaging.* 2003;17:323–329.
11. Hays WL. *Statistics.* Fort Worth: Harcourt Brace College Publishers; 1994.
12. Bomma C, Rutberg J, Tandri H, et al. Misdiagnosis of arrhythmogenic right ventricular dysplasia/cardiomyopathy. *J Cardiovasc Electrophysiol.* 2004;15:300–306.
13. Castillo E, Rutberg J, Wu KC, et al. Arrhythmogenic right ventricular dysplasia/cardiomyopathy: differences in protocols and image quality between MRI centers. *Radiology.* 2001 Nov; 221 Suppl:360.
14. Sievers B, Addo M, Franken U, et al. Right ventricular wall motion abnormalities found in healthy subjects by cardiovascular magnetic resonance imaging and characterized with a new segmental model. *J Cardiovasc Magn Reson.* 2004;6:601–608.
15. Marcus FI, Fontaine G. Arrhythmogenic right ventricular dysplasia/cardiomyopathy: a review. *Pacing Clin Electrophysiol.* 1995;18:1298–1314.
16. Thiene G, Basso C, Calabrese F, et al. Pathology and pathogenesis of arrhythmogenic right ventricular cardiomyopathy. *Herz.* 2000;25:210–215.
17. Auffermann W, Wichter T, Breithardt G, et al. Arrhythmogenic right ventricular disease: MR imaging vs angiography. *AJR Am J Roentgenol.* 1993;161:549–555.
18. Blake LM, Scheinman MM, Higgins CB. MR features of arrhythmogenic right ventricular dysplasia. *AJR Am J Roentgenol.* 1994;162:809–812.
19. Bluemke DA, Krupinski EA, Ovitt T, et al. MR imaging of arrhythmogenic right ventricular cardiomyopathy: morphologic findings and interobserver reliability. *Cardiology.* 2003;99:153–162.
20. Buxt LM, Rozenshtein A. MR imaging of arrhythmogenic right ventricular dysplasia. *Magn Reson Imaging Clin N Am.* 2003;11:163–171.
21. Midiri M, Finazzo M. MR imaging of arrhythmogenic right ventricular dysplasia. *Int J Cardiovasc Imaging.* 2001;17:297–304.
22. Tandri H, Saranathan M, Rodriguez ER, et al. Noninvasive detection of myocardial fibrosis in arrhythmogenic right ventricular cardiomyopathy using delayed-enhancement magnetic resonance imaging. *J Am Coll Cardiol.* 2005;45:98–103.
23. McKenna WJ, Thiene G, Nava A, et al. Diagnosis of arrhythmogenic right ventricular dysplasia/cardiomyopathy. Task Force of the Working Group Myocardial and Pericardial Disease of the European Society of Cardiology and of the Scientific Council on Cardiomyopathies of the International Society and Federation of Cardiology. *Br Heart J.* 1994;71:215–218.
24. Midiri M, Finazzo M, Brancato M, et al. Arrhythmogenic right ventricular dysplasia: MR features. *Eur Radiol.* 1997;7:307–312.